Hong Kong J Radiol. 2017;20:241-7 | DOI: 10.12809/hkjr1716860

PICTORIAL ESSAY

Cone-beam Computed Tomography for Transarterial Radioembolisation or Chemoembolisation of Hepatocellular Carcinoma

HF Chan, WH Luk, LF Cheng, JKF Ma

Department of Radiology, Princess Margaret Hospital, Lai Chi Kok, Hong Kong

ABSTRACT

Cone-beam computed tomography (CBCT) acquires three-dimensional volumetric images using a two-dimensional flat panel detector mounted on a C-arm that rotates around the patient. CBCT enables planning of transarterial radioembolisation or chemoembolisation by detection and analysis of small occult tumours, tumour-feeding arteries, and extrahepatic arterial feeders, and enables assessment of treatment outcome.

Key Words: *Carcinoma, hepatocellular; Chemoembolization, therapeutic; Cone-beam computed tomography*

中文摘要

錐形束電腦斷層掃描用於經動脈放療或化療栓塞治療肝細胞癌

陳可鋒、陸永恆、鄭力暉、馬嘉輝

錐形束電腦斷層掃描（CBCT）使用圍繞患者旋轉的C形臂上的二維平板檢測器獲取三維體積圖像。CBCT通過檢測和分析小隱匿性腫瘤、腫瘤供養動脈和肝外供養動脈來規劃經動脈放療或化療栓塞，並且評估治療結果。

INTRODUCTION

Cone-beam computed tomography (CBCT) acquires three-dimensional (3D) volumetric images using a two-dimensional flat panel detector mounted on a C-arm that rotates around the patient. CBCT angiography enables planning of transarterial chemoembolisation (TACE) and yttrium-90 (Y90) transarterial radioembolisation (TARE) by detection of small occult tumours, tumour-feeding arteries, and extrahepatic arterial feeders, and enables assessment of treatment outcome.[1,2] We report our experience in CBCT angiography for TARE or TACE of hepatocellular carcinoma (HCC).

PRINCIPLES

Conventional multi-detector computed tomography (MDCT) uses fan-beam geometry and a series of detector element rows.[3] CBCT uses cone-beam geometry and a two-dimensional flat panel detector mounted on a C arm to acquire 3D volumetric images.[3] The flat panel detector rotates around the patient, and

Correspondence: *HF Chan, Department of Radiology, Princess Margaret Hospital, Lai Chi Kok, Hong Kong.*
Email: chf178@ha.org.hk

Submitted: 17 Feb 2017; Accepted: 31 Mar 2017.

Disclosure of Conflicts of Interest: All authors have disclosed no conflicts of interest.

X-ray projection images are acquired along multiple angular directions, following a circular path covering ≥200°, which is the minimum required to fulfil the 180° plus the fan angle.[4] Images are then reconstructed to generate 3D volume data.

The isotropic voxel sizes of CBCT and MDCT are <0.2 x 0.2 x 0.2 mm^3 and 0.5 x 0.5 x 0.5 mm^3, respectively.[5] The spatial resolution is thus higher in CBCT than MDCT.[4] Higher spatial resolution enables delineation of tiny tumour-feeding arteries otherwise not discernible on MDCT,[5] particularly for superselective TACE. Nonetheless, the soft-tissue contrast resolution is lower in CBCT than MDCT (10 vs. 3 Hounsfield units),[5] because of increased beam scatter generated by the C-arm angiographic system.[6] CBCT in TACE can increase radiation exposure and the stochastic risk (dose-area product) of the procedure by 34%, but CBCT can replace some angiography runs and thus decrease the deterministic risk (cumulative dose) from digital subtraction angiography (DSA) by 50%.[7]

IMPLEMENTATION

Our centre uses the DynaCT system and the Artis intervention suite (both from Siemens Medical Solutions, Forchheim, Germany). CBCT is routinely used for treatment planning of Y90 TARE. For TACE, CBCT is used when conventional DSA fails to demonstrate the tumour that is detected in pre-procedural cross-sectional imaging or the tumour-feeding arteries that overlap with arterial branches, or when re-analysis of the tumour-feeding arteries is needed after unsatisfactory response to previous TACE treatment.

During CBCT, the patient is placed supine and any obstructing object along the path of the C-arm rotation is removed. A test run is performed before image acquisition. The patient is instructed to hold the breath for good-quality images and practise once before image acquisition.

CBCT angiography is obtained with the undiluted contrast (although 33% dilution is recommended by the manufacturer) injected through a 4- or 5-Fr catheter in the common hepatic artery or hepatic artery proper. Undiluted contrast enables better visualisation of tiny subsegmental hepatic arteries. If a 4- or 5-Fr catheter cannot be advanced into these arteries due to unstable celiac anatomy, then a 2.5- or 2.7-Fr microcatheter

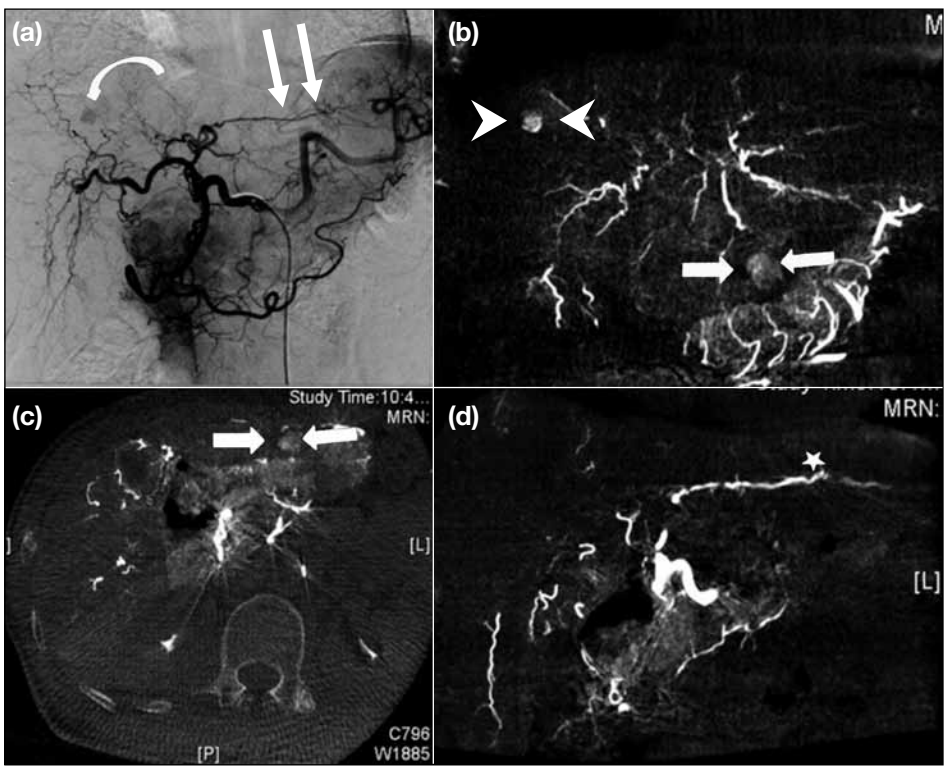

Figure 1. (a) Digital subtraction angiography of the liver showing a small hypervascular tumour at segment 4a (curved arrow) and an accessory left gastric artery from left hepatic artery at segment 2 (arrows), which should be avoided during chemoembolisation. (b-d) Cone-beam computed tomography angiography multiplanar-reformatted images showing the segment 4a tumour (arrowheads), the accessory left gastric artery from segment 2 artery (asterisk), and a previously missed tumour in segment 3 (arrows).

Figure 2. (a) Digital subtraction angiography of the liver showing a tiny area of vascularity at segment 6 (curved arrow) and a hypervascular tumour at the right lobe (arrow), but the exact location and arterial feeders of the tumour are not well delineated. (b, c) Cone-beam computed tomography angiography multiplanar-reformatted images showing the tumour's location at segment 7 (arrows) and arterial feeders from A7 (arrowheads). (d-f) Cone-beam computed tomography angiography volume-rendered images showing three-dimensional relationship of the arterial branches, the tumour at segment 7 (arrows), and its arterial feeders from A7 (arrowheads) by rotating the images into the right oblique direction. (g, j) Contrast-enhanced multi-detector computed tomography showing two tiny areas of arterial enhancement at the subcapsular region of segment 6 (arrow) and segment 7 (curved arrow) with no early washout. Both were considered as shunts or non-specific. (h, i, k, l) Intraprocedural cone-beam computed tomography angiography multiplanar-reformatted images showing the two discrete hypervascular nodular lesions at segment 6 (arrows) and segment 7 (arrowheads) suggestive of hepatocellular carcinomas. Both were targeted for chemoembolisation.

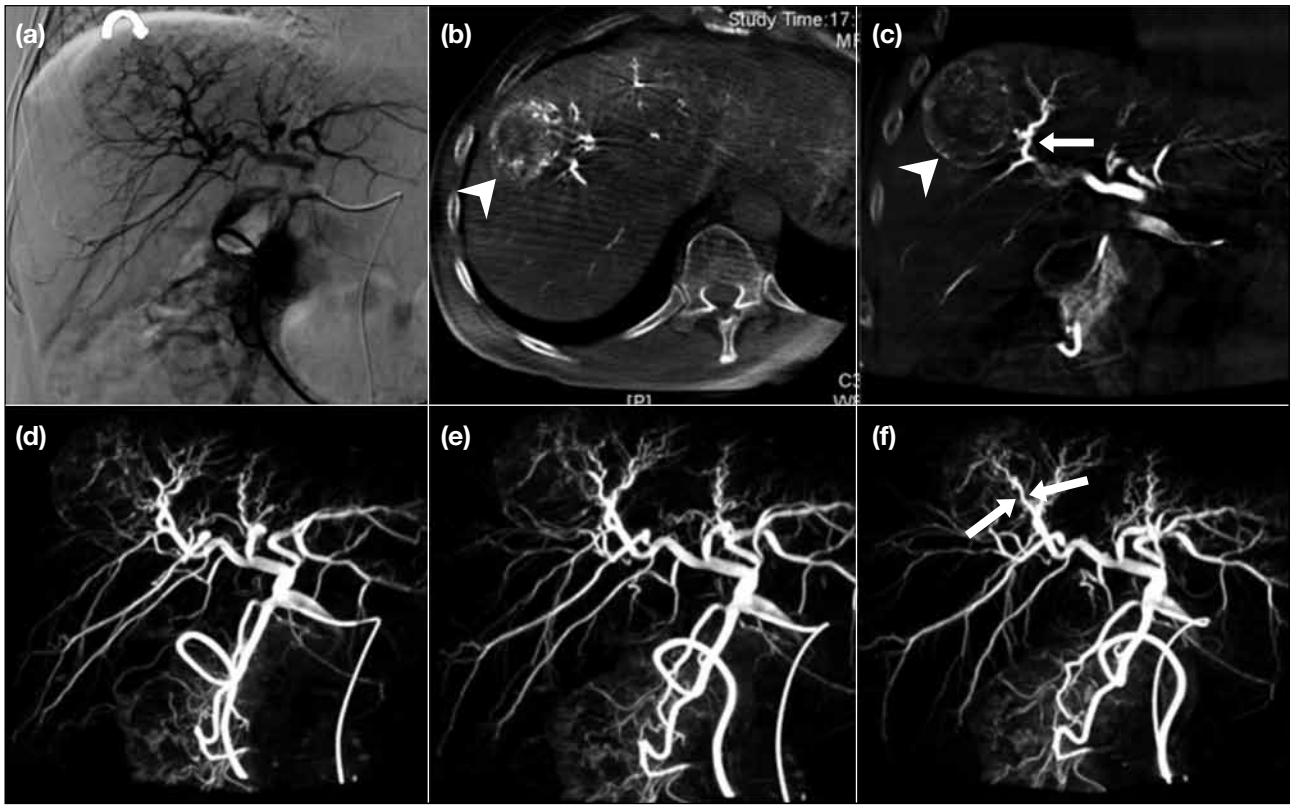

Figure 3. (a) Digital subtraction angiography of the liver showing vague vascularity (curved arrow) at segment 8 suggestive of a hypervascular tumour, but its feeding arteries are not well delineated due to overlapping arterial branches. (b, c) Cone-beam computed tomography angiography multiplanar-reformatted images showing the hypervascular tumour (arrowheads) and its feeding arteries (arrow) clearly. (d-f) Cone-beam computed tomography angiography maximum intensity projection volume-rendered images rotating in an oblique direction showing the three-dimensional relationship of overlapping arteries and the feeding artery (arrows).

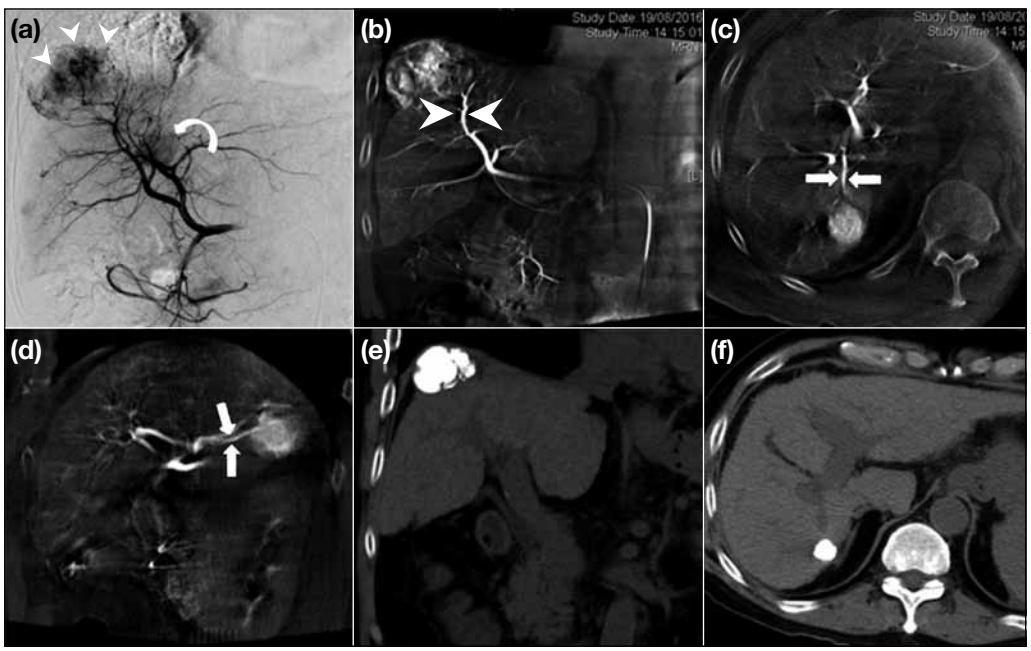

Figure 4. (a) Digital subtraction angiography of the liver showing hepatocellular carcinomas at segment 8 (arrowheads) and segment 7 (curved arrow), but the A8 and A7 arterial branches are overlapped and the feeding arteries not delineated. (b-d) Cone-beam computed tomography angiography multiplanar-reformatted images showing the tumour-feeding arteries at segment 8 (arrowheads) and segment 7 (arrows). (e, f) Follow-up computed tomography showing dense lipiodol retention and shrinkage in both tumours suggestive of successful chemoembolisation.

Figure 5. (a) Digital subtraction angiography of the liver following transarterial chemoembolisation showing a residual viable tumour at segment 8 and two possible feeding arteries (arrowhead and arrow) and partial lipiodol retention. (b, c) Cone-beam computed tomography angiography maximum intensity projection volume-rendered images showing the two possible feeding arteries (arrowhead and thin arrow) and the correct feeding artery (thick arrow). (d, e) Cone-beam computed tomography angiography multiplanar-reformatted images showing a non-enhancing area at the targeted tumour at segment 8 (arrows) suggestive of extrahepatic arterial supply. (f, g) The ascending superior branch of the right inferior phrenic artery is chemoembolised using a 2-Fr microcatheter (arrowhead) (h, i) Follow-up computed tomography showing a dense lipiodol-stained tumour suggestive of successful chemoembolisation.

is used. A total volume of 30 to 40 ml of contrast is injected at a rate of 3 to 4 ml per second. The scan delay time is 3 to 4 seconds, which is similar to 3 to 6 seconds reported in other centres.[1,8] A shorter delay (3 seconds) enables better visualisation of the hepatic artery, whereas a longer delay (6 seconds) enables better visualisation of small tumours.

CBCT images including multiplanar-reformatted and maximum intensity projection images are reviewed by the interventional radiologist inside the intervention suite (Figures 1 to 7).

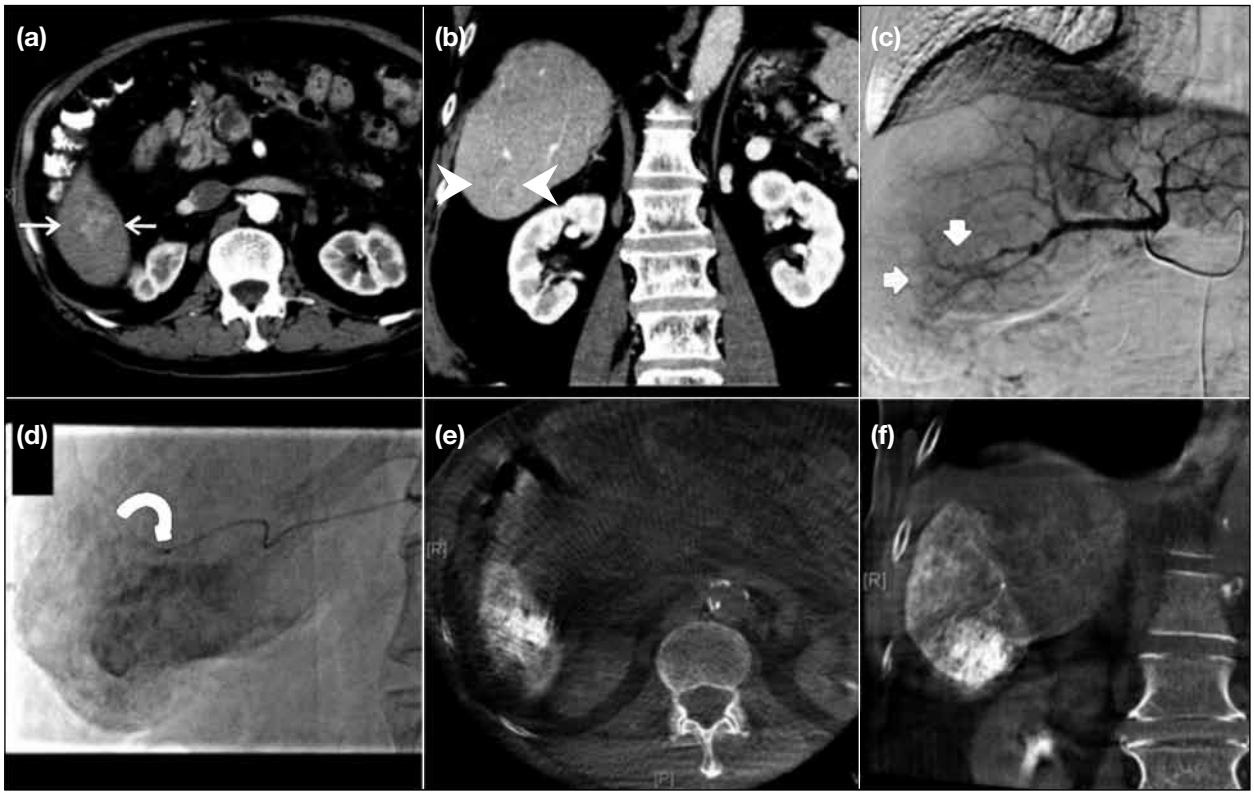

Figure 6. (a, b) Contrast-enhanced multi-detector computed tomography showing an area of ill-defined arterial enhancement at segment 6 (arrows) and early washout in the portovenous phase (arrowheads). (c, d) Digital subtraction angiography showing equivocal vascularity at segment 6 (arrows) and no identifiable tumour-feeding artery. Chemoembolisation is empirically performed at A6 using a 2-Fr microcatheter (curved arrow). (e, f) Cone-beam computed tomography showing dense lipiodol accumulation in the tumour confirming adequate chemoembolisation.

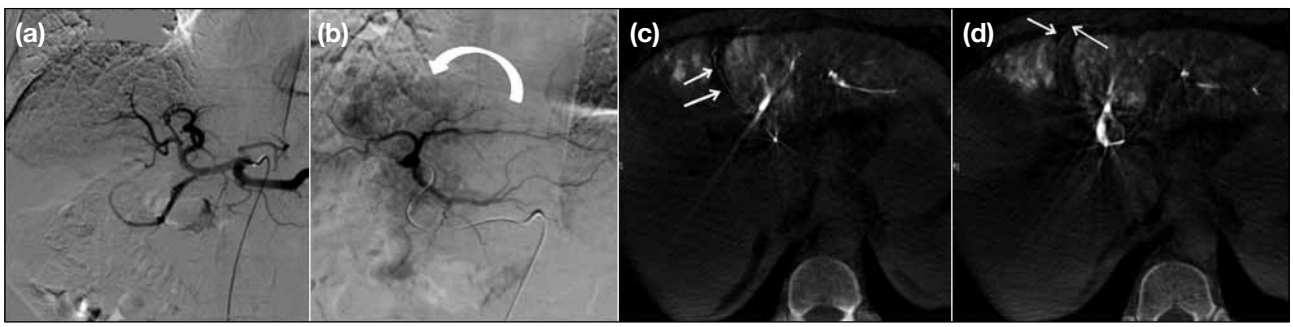

Figure 7. (a, b) Digital subtraction angiography of the liver showing the celiac trunk and left hepatic artery, and a hypervascular tumour in the left lobe (curved arrow). (c, d) Cone-beam computed tomography angiography showing the artery of the falciform ligament originating from the previously missed left hepatic artery (arrows), which is coil-embolised to prevent injury to the abdominal wall due to non-targeted yttrium-90 radioembolisation.

DISCUSSION

CBCT is more sensitive than MDCT and DSA in the detection of small occult HCC (<2 cm) because of its superior spatial resolution.[9,10] However, CBCT is less specific than MDCT and DSA in differentiating other benign hypervascular lesions such as vascular shunt and hepatic haemangioma that mimic HCC.[11]

The higher spatial resolution of CBCT angiography enables delineation of subsegmental tumour-feeding arteries that are not discernible by MDCT. Compared with DSA, CBCT angiography better demonstrates the

3D configuration of the feeding arteries, as the arterial branches often appear overlapping with each other in DSA. Sensitivity, specificity, and accuracy are higher in CBCT than DSA in terms of identification of tumour-feeding arteries.[12,13]

Large or peripherally located HCCs are frequently supplied by both intrahepatic and extrahepatic arterial feeders that should be identified and embolised early for effective TACE. If part of the tumour is not enhanced in CBCT angiography, then an extrahepatic arterial feeder is suggested and further investigation should be made.[14]

CBCT immediately after chemoembolisation provides instant feedback about the adequacy of chemoembolisation. The treatment goal is to chemoembolise the entire target tumour with a safety margin.[5] The catheter position can be adjusted for further chemoembolisation. CBCT is comparable with MDCT in detecting incomplete iodised oil accumulation after chemoembolisation.[15] Intraprocedural monitoring of the chemoembolised area can reduce the risk of local recurrence.[16]

In planning of Y90 TARE, in addition to DSA and technetium 99m–labelled macro-aggregated albumin scintigraphy, CBCT angiography can detect arteries not seen by DSA to avoid potential non-target embolisation.

CONCLUSION

CBCT enables detection of small occult tumours, tumour-feeding arteries, and extrahepatic arterial feeders for treatment planning, and enables assessment of treatment outcome.

REFERENCES

1. Wallace MJ, Kuo MD, Glaiberman C, Binkert CA, Orth RC, Soulez G, et al. Three-dimensional C-arm cone-beam CT: applications in the interventional suite. J Vasc Interv Radiol. 2009;20(7 Suppl):S523-37. cross ref
2. Louie JD, Kothary N, Kuo WT, Hwang GL, Hofmann LV, Goris ML, et al. Incorporating cone-beam CT into the treatment planning for yttrium-90 radioembolization. J Vasc Interv Radiol. 2009;20:606-13. cross ref
3. Orth RC, Wallace MJ, Kuo MD; Technology Assessment Committee of the Society of Interventional Radiology. C-arm cone-beam CT: general principles and technical considerations for use in interventional radiology. J Vasc Interv Radiol. 2008;19:814-20. cross ref
4. Hirota S, Nakao N, Yamamoto S, Kobayashi K, Maeda H, Ishikura R, et al. Cone-beam CT with flat-panel-detector digital angiography system: early experience in abdominal interventional procedures. Cardiovasc Intervent Radiol. 2006;29:1034-8. cross ref
5. Kim HC. Role of C-arm cone-beam CT in chemoembolization for hepatocellular carcinoma. Korean J Radiol. 2015;16:114-24. cross ref
6. Bapst B, Lagadec M, Breguet R, Vilgrain V, Ronot M. Cone beam computed tomography (CBCT) in the field of interventional oncology of the liver. Cardiovasc Intervent Radiol. 2016;39:8-20. cross ref
7. Kothary N, Abdelmaksoud MH, Tognolini A, Fahrig R, Rosenberg J, Hovsepian DM, et al. Imaging guidance with C-arm CT: prospective evaluation of its impact on patient radiation exposure during transhepatic arterial chemoembolization. J Vasc Interv Radiol. 2011;22:1535-43. cross ref
8. Tognolini A, Louie JD, Hwang GL, Hofmann LV, Sze DY, Kothary N. Utility of C-arm CT in patients with hepatocellular carcinoma undergoing transhepatic arterial chemoembolization. J Vasc Interv Radiol. 2010;21:339-47. cross ref
9. Iwazawa J, Ohue S, Hashimoto N, Abe H, Hamuro M, Mitani T. Detection of hepatocellular carcinoma: comparison of angiographic C-arm CT and MDCT. AJR Am J Roentgenol. 2010;195:882-7. cross ref
10. Miyayama S, Yamashiro M, Okuda M, Yoshie Y, Sugimori N, Igarashi S, et al. Usefulness of cone-beam computed tomography during ultraselective transcatheter arterial chemoembolization for small hepatocellular carcinomas that cannot be demonstrated on angiography. Cardiovasc Intervent Radiol. 2009;32:255-64. cross ref
11. Meyer BC, Frericks BB, Voges M, Borchert M, Martus P, Justiz J, et al. Visualization of hypervascular liver lesions during TACE: comparison of angiographic C-arm CT and MDCT. AJR Am J Roentgenol. 2008;190:W263-9. cross ref
12. Iwazawa J, Ohue S, Mitani T, Abe H, Hashimoto N, Hamuro M, et al. Identifying feeding arteries during TACE of hepatic tumors: comparison of C-arm CT and digital subtraction angiography. AJR Am J Roentgenol. 2009;192:1057-63. cross ref
13. Meyer BC, Witschel M, Frericks BB, Voges M, Hopfenmüller W, Wolf KJ, et al. The value of combined soft-tissue and vessel visualisation before transarterial chemoembolisation of the liver using C-arm computed tomography. Eur Radiol. 2009;19:2302-9. cross ref
14. Tacher V, Radaelli A, Lin M, Geschwind JF. How I do it: cone-beam CT during transarterial chemoembolization for liver cancer. Radiology. 2015;274:320-34. cross ref
15. Iwazawa J, Ohue S, Kitayama T, Sassa S, Mitani T. C-arm CT for assessing initial failure of iodized oil accumulation in chemoembolization of hepatocellular carcinoma. AJR Am J Roentgenol. 2011;197:W337-42. cross ref
16. Miyayama S, Yamashiro M, Hashimoto M, Hashimoto N, Ikuno M, Okumura K, et al. Comparison of local control in transcatheter arterial chemoembolization of hepatocellular carcinoma ≤6 cm with or without intraprocedural monitoring of the embolized area using cone-beam computed tomography. Cardiovasc Intervent Radiol. 2014;37:388-95. cross ref